Article

Seismic Performance of an Exterior Joint between a Square Steel Tube Column and an H-Shape Steel Beam

Yongle Lin [1], Xinwu Wang [2,*], Jian Gong [1], Shuren Wang [1,3], Haisu Sun [2] and Huanhuan Liu [2]

1   College of Civil Engineering, Henan Polytechnic University, Jiaozuo 454003, China
2   Henan International Joint Laboratory of New Civil Engineering Structure, Luoyang 471023, China
3   International Joint Research Laboratory of Henan Province for Underground Space Development and Disaster Prevention, Henan Polytechnic University, Jiaozuo 454003, China
*   Correspondence: lywxw518@163.com

Abstract: This study developed a 1:2 scale model using T-shape steel with one-side bolts to connect a square steel tube column to an H-shape steel beam for a quasi-static test to investigate the mechanical properties and seismic behavior of semi-rigid joints. Within the study context, the joint's failure characteristics, hysteresis characteristics, and strain tendency under cyclic load were determined. In addition, this research analyzed the force characteristics and seismic performance of such joints based on the test outcomes. In order to further study the seismic performance of such joints, ABAQUS finite element software was used to establish a numerical model and perform parametric analysis. The findings indicated that the force on both sides of the joint is inconsistent, resulting in different seismic performances on both sides of the joint. Selecting a T-shape steel connector significantly affects the seismic capacity of beam–column joints. The seismic capacity of joints can be improved by increasing the size of the T-shape steel. The stability of one-side bolts under repeated load is good, and their strain value rises steadily. Hence, this type of one-side bolt is suitable for connecting closed steel tube columns and other components. In general, the seismic performance of square steel tube column–H-shape steel beam joints with one-side bolts and a T-shape steel connection is good and is recommended for practical engineering.

Keywords: one-side bolts; quasi-static test; hysteresis characteristics; seismic performance

1. Introduction

Prefabricated buildings can be divided into concrete structures, steel structures, modern wood structures, and others. The use of steel buildings in construction has grown rapidly due to the advantages of green environmental protection, short construction period, and good seismic resistance. Among forms of connection for steel beam–column joints, the semi-rigid connection can withstand a specific bending moment and a particular rotation, making it an ideal connection method in steel structures. Wang Xinwu et al. analyzed the failure morphology and energy dissipation mechanism of such connections. They showed that the semi-rigid connection steel frame has good seismic performance and engineering application value [1].

Square steel column and H-shape steel beam in semi-rigid beam–column joints are the two main stress components commonly used in multi-story and high-rise steel structure buildings [2]. The square steel column solves the effect of the difference between the solid and weak axes of the H-shape column section and the force in various directions, thereby ensuring structural stiffness. Standard high-strength bolts cannot be used directly for these connections. One-side bolts can be tightened in one direction, and it is not necessary to drill a hand hole in the column wall in order to operate the bolt without damaging the column. One-side bolts are also convenient for on-site construction and beam–column connection. Many scholars have conducted in-depth studies on one-side bolts [3–9].

Wang Yan et al. investigated the failure mode and tensile ultimate bearing capacity of one-side high-strength bolts. They demonstrated that the tensile ultimate bearing capacity of one-side high-strength bolts is the same as that of conventional high-strength bolts [10]. He Zefeng et al. examined the similarities and differences in the seismic performance of a new one-side all-bolt joint and a typical all-bolt joint by comparing two test sets. The results showed that the seismic performance of both test groups was comparable [11]. Lee evaluated the mechanical properties of steel pipe joints connected to one-side bolts. The analysis revealed that the new one-side bolts provide a reliable connection for low-rise buildings [12].

This study conducts a quasi-static test on a specimen of T-shape steel with one-side bolts to connect a square steel tube column to H-shape steel beam joints and derives the hysteresis curve for the joint. It comprehensively analyzes the seismic characteristics of the joints by comparing the force difference between the east beam and the west beam and verifies the superiority of such joints in practical engineering. By analyzing the degree of breakage of and strain on one-side bolts, the applicability of using such one-side bolts to connect closed steel pipe columns is verified. Moreover, the data presented in this study provide a reference for the application of these beam–column joints.

2. Test Overview

2.1. Component Design

The test model was a 1:2 scale representation of the joint of a multi-story steel frame structure. The test model adopted the design principle of strong column and weak beam to improve the deformation capacity of the structure. The middle column joint test model was designed and manufactured according to the requirements of 'Steel Structure Design Standard' (GB50017-2017) and 'Code for Seismic Design of Buildings' (GB50011-2010). The column was a Q235B grade square steel column with a 10 mm thick rib plate added to the column and beam flange cross-section alignment. The beam and T-shape steel were hot-rolled steel of Q235B grade. Table 1 lists the specific section sizes. Two bolts were used for test piece connection: 10.9-grade M16 friction-type high-strength bolts (connected T-shape steel web to beam flange) and 10.9-grade M16 nested one-side bolts (connected T-shape steel flange to column wall). The connection and installation of each component in the test were strictly conducted following the 'Code for Acceptance of Construction Quality of Steel Structures' (GB50205-2020) [13]. Figures 1–3 depict the specimen model and size.

Table 1. Cross-sectional dimensions of members.

Component	Cross-Sectional Dimensions/mm	Grade
Column	$200 \times 10 \times 10$	Q235B
Beam	HN $250 \times 125 \times 6 \times 9$	Q235B
T-shape steel	HN $210 \times 170 \times 9 \times 14$	Q235B
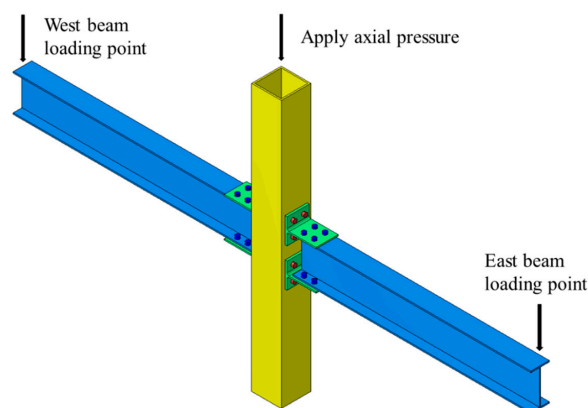
Figure 1. Specimen model.

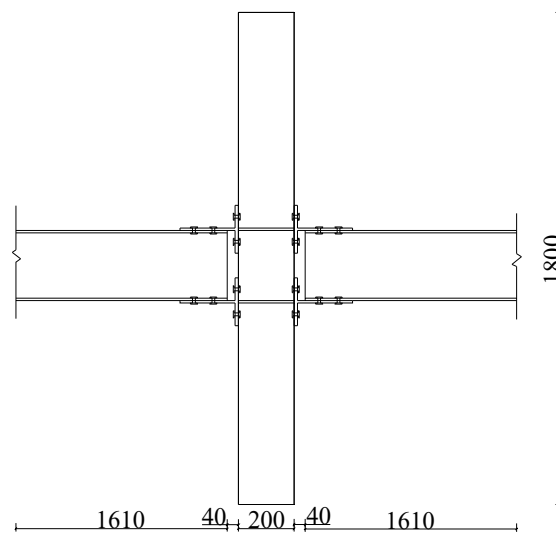**Figure 2.** Overall size (mm).

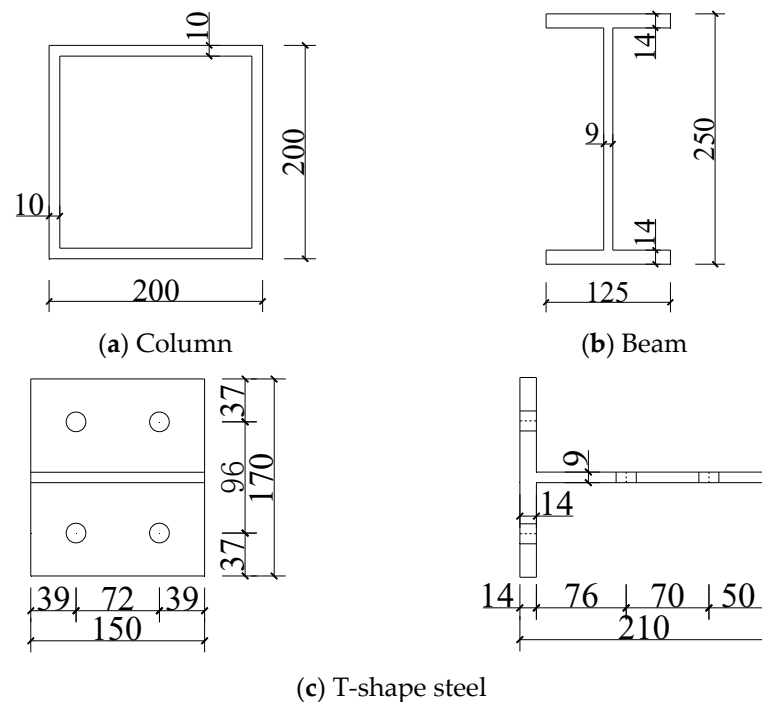

(**a**) Column

(**b**) Beam

(**c**) T-shape steel

Figure 3. Section size of each component (mm).

M16-type nested one-side bolts were used in this test (Figure 4). The bolt head was connected to the column wall. The bolt sleeve was placed between the bolt hole in the column wall, and the sleeve length did not exceed the column wall thickness. Owing to the sleeve's large outer diameter, the surface opening diameter for the one-side bolt connection member was 24 mm, and the sleeve length after processing was 9 mm. However, according to the results of a previous study on the mechanical properties of one-side bolts, it is evident that during the proposed static test with cyclic loading, the nut part of the one-side bolts connecting the T-shape steel flange sinks deep into the bolt hole due to the loading process. This causes plastic deformation of the T-shape steel flange in advance, resulting in component failure. Therefore, the opening diameter of the one-side bolt connection to the T-shape steel flange was 17.5 mm. The hole shape for the column wall bolt varied from that of the T-shape steel flange bolt, as revealed in Figure 5. This satisfies the installation

requirements of one-side bolts and expands the force area of one-side bolts at the T-shape steel flange.
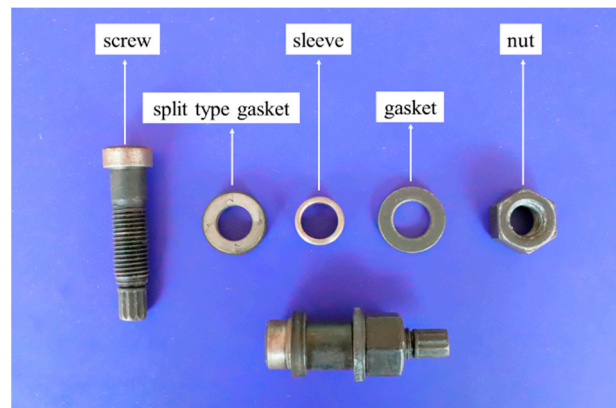

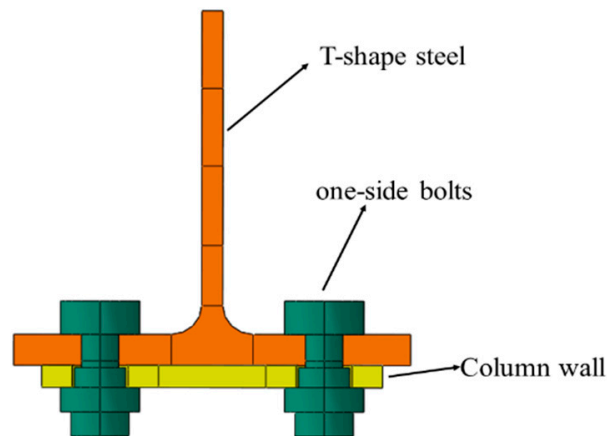**Figure 4.** One-side bolts.

Figure 5. Different holes.

2.2. Material Properties Test

Before the test, the theoretical values for the yield strength and ultimate strength of steel were obtained by testing the mechanical properties of each component at different thicknesses using the GB/T288.1-2010 standard [14]. Figure 6 illustrates the tensile test specimens, and Table 2 displays the mechanical property test results. The standard deviations of each value in Table 2 are within 20%, which meets the requirements.


Figure 6. Tensile test specimens.

Table 2. Mechanical properties of specimen materials.

Component	t/mm	f_y/MPA	f_u/MPA	E/GPA	δ/%	εy/%
Column	10	345	491	209	30.3	0.165
Beam	6	280	442	196	34.5	0.143
	9	252	440	199	32.2	0.127
T-shape steel	9	289	463	207	30.7	0.148
	14	269	447	197	33.0	0.136

2.3. Test Device

The loading method at the beam end in the proposed static test of the beam–column connection joint matches the joint's force state to the actual one. The beam end loading approach was selected for the test, and Figure 7 shows the test site. The column's top was connected using a 200 t vertical actuator, while the bottom was connected using a single knife hinge support. The hinge support was fixed to the rigid ground by anchor bolts. The east and west beams were connected to the vertical east 100 t actuator and west 100 t actuator, respectively, at the loading end. The actuators at the east and west ends utilized a guide screw and a lattice column as constraint devices to prevent lateral specimen displacement during the loading process.
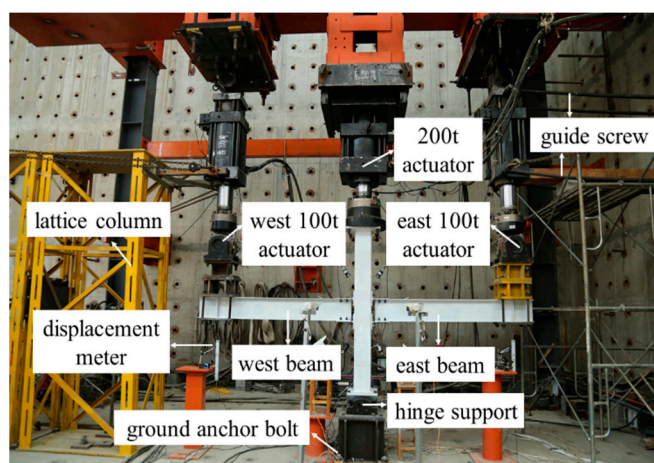

Figure 7. Field device diagram.

3. Test Scheme

3.1. Loading System

The test utilized a dual-control load–displacement approach based on the JGJ/T101-2015 standard [15]. The specimen was load controlled before yielding. Thereafter, the load control was changed to a displacement control when the specimen's strain reached the mechanical property test yield value. Displacement loading was performed with an integer in multiples of the yield displacement. Figure 8 shows the test loading regime curve. An axial pressure of 310 KN was applied to the top of the specimen column using the vertical 200 t actuator to simulate the column's axial pressure. In addition, the axial pressure was guaranteed to remain constant throughout the test. When the specimen was stable under an axial compression load, vertical load–displacement control was applied at the loading end of the cantilever beam. The actuator considered push to be the positive load and pull to be the negative load. The east 100 t vertical actuator was utilized to apply positive load control to the east beam end, and the west 100 t actuator applied reverse load control to the west beam end. The east and west actuators were inducing load synchronously, and the synchronization was reset to zero once the loading was complete. The actuator's positive and negative loading process was one complete cyclic loading. Each loading grade was

loading for three cycles until the component was damaged or the bearing capacity fell below 85% of the specimen's ultimate load. Then, the test was terminated.
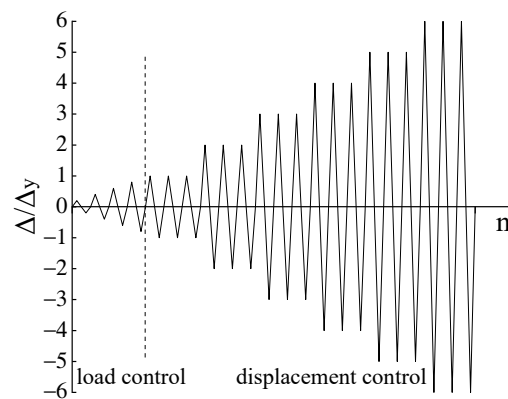

Figure 8. Loading system diagram.

3.2. Measurement Solution

The test was conducted using beam-end loading. A needle displacement meter was set vertically at the lower part of the east beam loading end and the west beam loading end to measure the displacement data for the beam ends during the loading process. A needle displacement meter was located in the horizontal direction of the column bottom to observe the displacement of the column during the loading process. A cable displacement meter was arranged around the joint to measure the deformation and obtain the joint's relative rotation angle. The rotation angle was calculated using Equation (1):

$$\cos(\,90° + \,\alpha) = \frac{(c+d)^2 - \left(\,a^2 + b^2\right)}{2} \tag{1}$$

where α is the relative angle of the beam and column; d is the reading of the cable displacement meter; and a and b are the distance between the two ends of the cable displacement meter and the column flange and the beam flange, respectively. a, b, and c form a right-angled triangle; a and b are the two sides of a right triangle; and c is the triangle's hypotenuse.

Figure 9 depicts the displacement meter positioning. In order to accurately monitor the specimen's deformation development during the test, a strain gauge and the strain flower were placed on each component at appropriate positions. Figure 10 shows the specific arrangement.
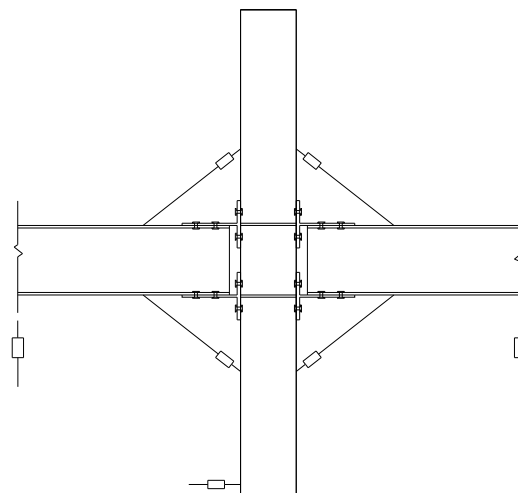
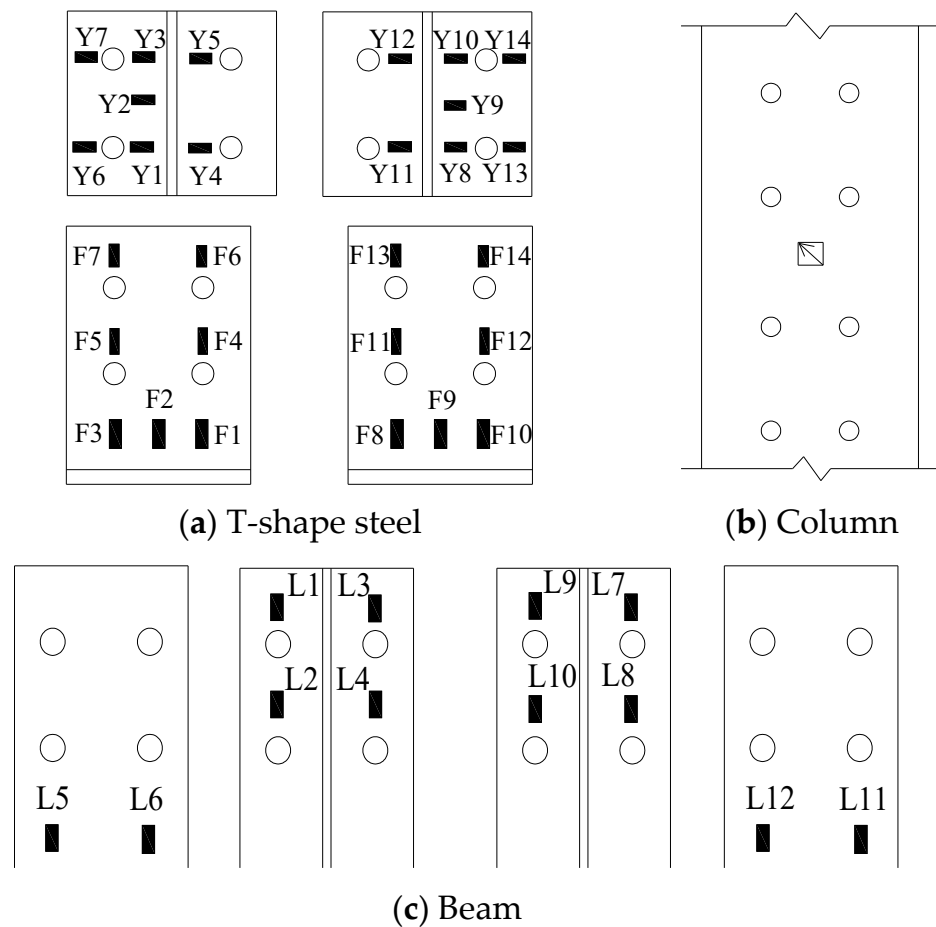
**Figure 9.** Layout of displacement meters.

(a) T-shape steel   **(b)** Column

(c) Beam

Figure 10. Layout of strain gauges.

4. Test Phenomena

As mentioned previously, the test was load controlled in the early stage. When the west 100 t actuator was loaded to 21 kN in the negative direction, the outer flange of the west beam lower T-shape steel (tensioned side) on the flange and the flange–web junction were the first to reach yield. At this time, the yield displacement of the specimen was about 17.3 mm. After that, the actuator was loaded using a displacement-controlled protocol, and the cyclic loading began with the 17.3 mm yield displacement as 1Δ. At this stage, there was no apparent phenomenon after 1Δ loading. On the other hand, when loading to 2Δ, the T-shape steel flange on the tension side began to be pulled away from the column wall and the gap gradually enlarged (Figure 11a). After loading to 3Δ on the first cycle, the tensile side of the east beam flange yielded a 2 mm maximum gap between the tensile side of the T-shape steel flange and the column wall. When loading to 5Δ, buckling occurred at the intersection of the T-shape steel web and the beam end flange below the east beam (Figure 11b). Two tiny cracks appeared at the T-shape steel web and flange junction, and a slight buckling occurred at the junction of the T-shape steel web below the west beam and the flange of the beam end. In addition, there were small cracks of about 11 mm at the junction of the T-shape steel web and the flange. Some tiny cracks appeared at the junction of the T-shape steel web and flange on the upper part of the west beam. The gap between the T-shape steel on the tension side and the column wall was about 5 mm. After loading to 6Δ on the third cycle, the cracks widened at each place and extended to the sides (Figure 11c). The buckling was more evident at the junction of the beam with the T-shape steel. After loading to 6Δ on the fourth cycle, plastic fracture occurred at the junction of the T-shape steel flange and the web in the lower part of the east beam. Figure 11d depicts the damage phenomenon. At this point, the test was terminated.

(**a**) Pull away

(**b**) Buckling

(**c**) Crack

(**d**) Fracture
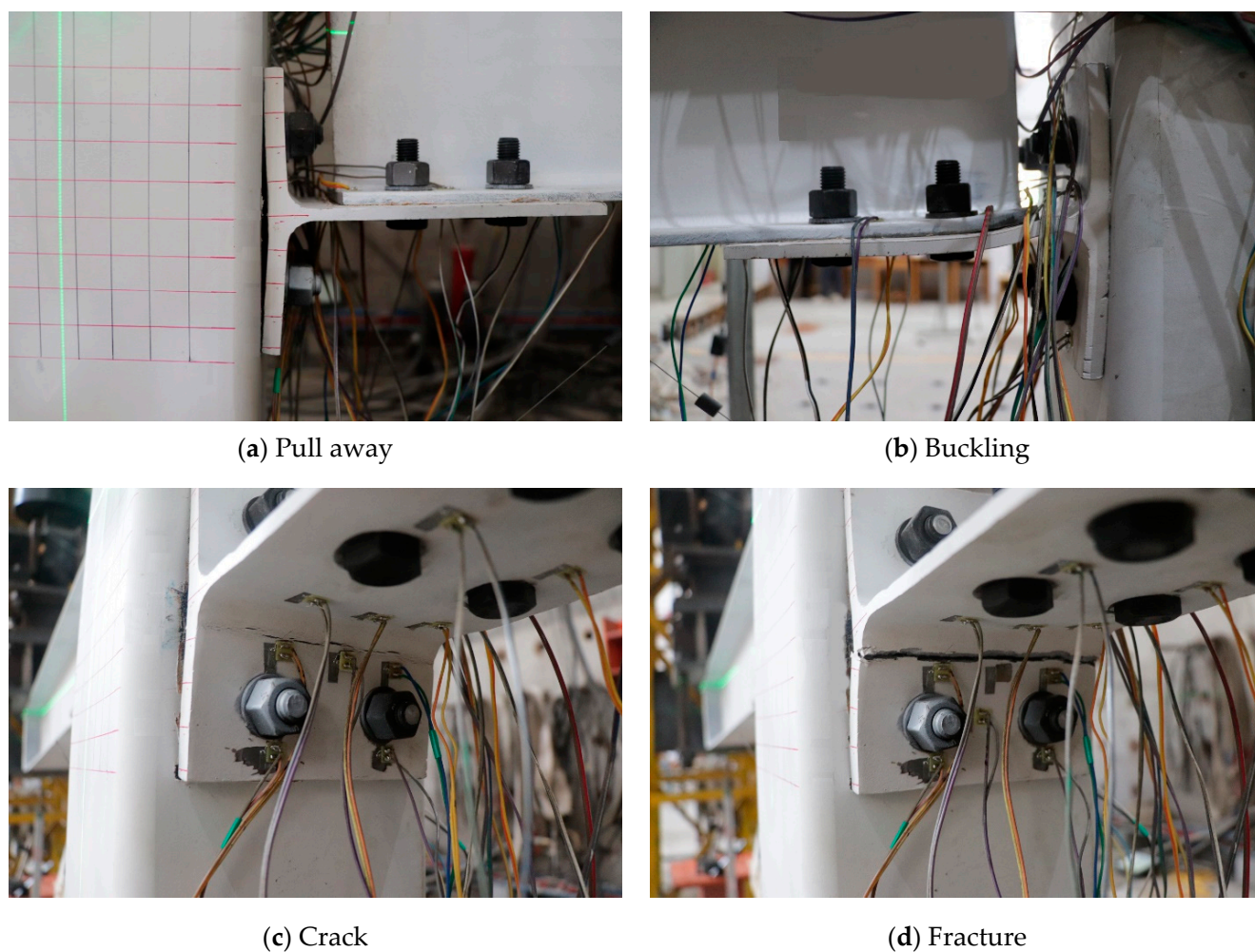
Figure 11. Test phenomena.

5. Test Results and Analyses

5.1. Test Results

Table 3 lists the test results. Comparing the test results of the east and west beams, the positive and negative yield displacements were consistent with the ultimate displacements. The specimen maintained a relatively stable state during the test loading process. The positive yield-bearing capacity of the east beam and ultimate bearing capacity were, respectively, 8.2% and 9.0% larger than those of the west beam. The negative yield-bearing capacity of the east beam was 19.3% smaller than that of the west beam, whereas the ultimate bearing capacity was 4.4% larger than that of the west beam. During the loading process, as the bolt preloading force decreased, the distance between the column wall and the T-shape steel flange continued to increase, resulting in different degrees of T-shape steel side torsion.

Table 3. Test results.

Beam Position	Yield Stage		Limit Stage	
	Displacement/mm	Load/KN	Displacement/mm	Load/KN
east	17.24	30.09	104.52	72.15
	−17.29 [1]	−17.13	−103.92	−66.13
west	17.25	27.80	103.88	67.41
	−17.27	−21.23	−103.82	−63.32

[1] A negative sign in the table indicates that the loading direction is negative.

### 5.2. Hysteretic Characteristics

Figure 12 shows the hysteresis curve for the test beam's loading end. Both curves were inverted S-type, exhibiting an apparent pinching phenomenon. The positive and negative bearing capacity differences could be caused by (1) material defects and uneven steel properties; (2) gaps in the connection between each component and the actuator, and construction errors; and (3) the specimen experiencing forward and reversed tension force states, resulting in the Bauschinger effect and a difference between the positive and negative bearing bending moments [16]. Generally, the hysteresis curves of the east and west beams have a high degree of fit. The seismic performance of both joint sides under repeated loads is essentially identical.
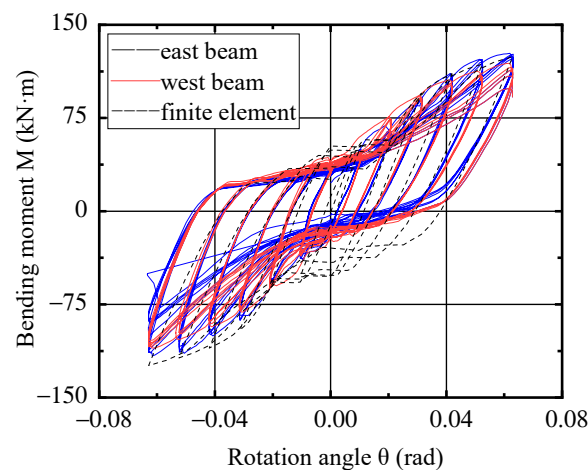
Figure 12. Hysteresis curve.

5.3. Skeleton Curve

The skeleton curve represents the force and deformation characteristics of the joints at different loading stages. Figure 13 shows the skeleton curves for the east and west beams. During the initial stage, the positive bending moment of the east and west beams was identical. The negative bending moment of the east beam was less than that of the west beam. This is primarily due to each component's continuous contact and running-in at the initial loading stage, resulting in differences in bearing capacity. After the third loading stage, the flexural bearing capacity of the east beam was gradually greater than that of the west beam until the end of the test. This was because, as the load rises, the degree of plastic deformation of the T-shape steel on the east and west sides was slightly different, so the force of the east and west beam ends varied.
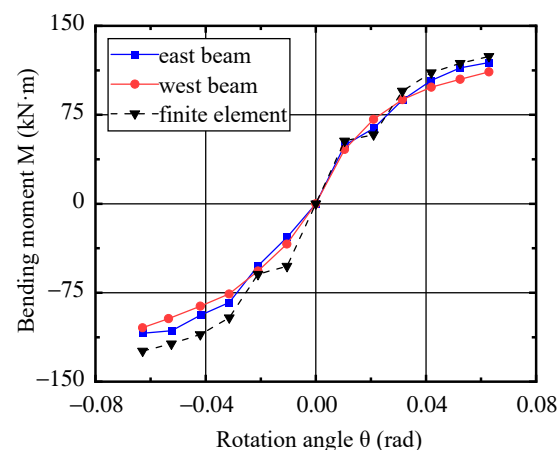
Figure 13. Skeleton curve.

5.4. Analysis of Rotational Stiffness Degradation

The rotational stiffness degradation represents the joints' seismic performance under cyclic load. In this paper, secant stiffness was employed to represent the stiffness variation of the joint under each loading stage. The secant stiffness is the ratio of the sum of the absolute values of the positive and negative maximum bending moments to the sum of the absolute values of the corresponding rotation angles at the same stage. The calculation formula is:

$$k_i = \frac{|+M_i| + |-M_i|}{|+\theta_i| + |-\theta_i|} \tag{2}$$

where M_i is the peak bending moment under the i-stage cyclic load and θ_i is the rotation angle corresponding to the peak bending moment under the i-stage cyclic load.

Figure 14 indicates that the stiffness of the west beam was slightly larger than that of the east beam at the initial stage of the test loading. At the later stages of the test loading, the stiffness of the east beam gradually exceeded that of the west beam. The stiffness degradation curves of both beams intersected between the second and third loading stages. During the test loading process, the stiffness degradation trend of the east and west beams was relatively stable, and the stiffness degradation curves of the two were approximately linear. In general, the stiffness difference between the east beam and the west beam was between 2.7% and 9.9%, and the overall stiffness of the joint was good.
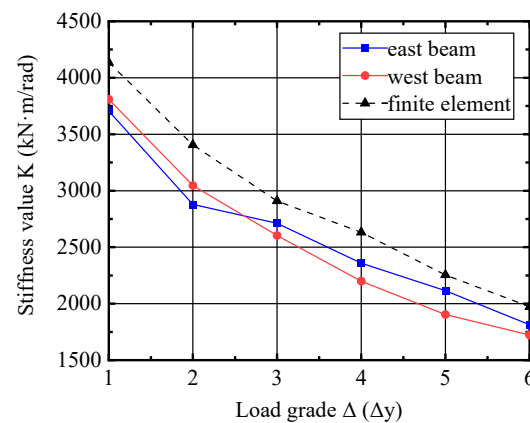

Figure 14. Rotational stiffness degradation curve.

5.5. Ductility

The ductility coefficient is essential for determining the specimens' plastic deformation capacity. The ductility coefficient is equal to the ratio of the ultimate rotation angle to the yield rotation angle. The yield rotation angle was calculated using the equivalent elastic stiffness method. Table 4 shows the joints' ductility factors. Based on the table, overall joint ductility was good. The ductility coefficient of the east and west beams was about 2.5, the ductility coefficient of the west beam was 1.6% less than that of the east beam, and the error was minor.

Table 4. Ductility coefficient.

| The Beam Number	θ_y/mrad	θ_u/mrad	μ
East	25.22	63.09	2.51
West	25.47	62.91	2.47

5.6. Energy Dissipation Capacity

The energy dissipation capacity indicates the structure's seismic performance under cyclic load. The energy dissipation capacity of the structure is usually evaluated using the cumulative energy dissipation, energy dissipation coefficient, and equivalent viscous

damping coefficient. In this test, the area of the first hysteresis loop in the specimen's last load stage was used as the cumulative energy dissipation. Figure 15 is the calculation diagram for the equivalent viscous damping coefficient h_e. Formulas (3) and (4) were used to calculate h_e and E, respectively. Table 5 lists the energy dissipation parameters (W is cumulative energy dissipation; E is energy dissipation coefficient; h_e is equivalent viscous damping coefficient). Based on the coefficients in the table, the equivalent viscous damping coefficient of the east and west beams was greater than 0.16, and the joint's energy dissipation capacity was adequate. The cumulative energy dissipation coefficient, energy dissipation coefficient, and equivalent viscous damping coefficient of the east beam were lower than those of the west beam by 0.8%, 13.2%, and 13.4%, respectively. The difference in force between the east and west sides during the test loading process was the primary cause. The bolts on the east beam slipped in advance, making the pinching phenomenon more obvious. Hence, the energy dissipation capacity of the east beam was slightly worse.

$$h_e = \frac{1}{2\pi} \frac{S_{(ABC+CDA)}}{S_{OBE} + S_{ODF}} \tag{3}$$

$$E = \frac{S_{(ABC+CDA)}}{S_{OBE} + S_{ODF}} \tag{4}$$
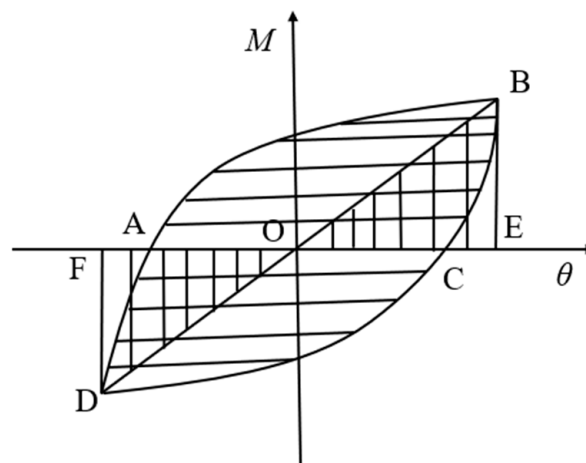
Figure 15. Calculation diagram of equivalent viscous damping coefficient.

Table 5. Energy dissipation capacity.

Beam Position	W	E	h_e
East	7.35	1.014	0.161
West	7.41	1.169	0.186

In Equations (3) and (4), $S_{(ABC+CDA)}$ is the area of the hysteresis loop ABCD; S_{OBE} is the area of triangular OBE; and S_{ODF} is the area of triangular ODF.

6. Finite Element Analysis

ABAQUS finite element software was used for modelling, and the model size and loading system were consistent with the test. The model components are meshed by a hexahedral element shape and numerically simulated by 8-node linear element C3D8I. The Von Mises yield criterion is used in the model analysis, and the mechanical properties are shown in Table 2. The plane center points of the column top, column foot, and beam loading end are set as reference points to a couple and constrain their degrees of freedom. The finite element model is shown in Figure 16.
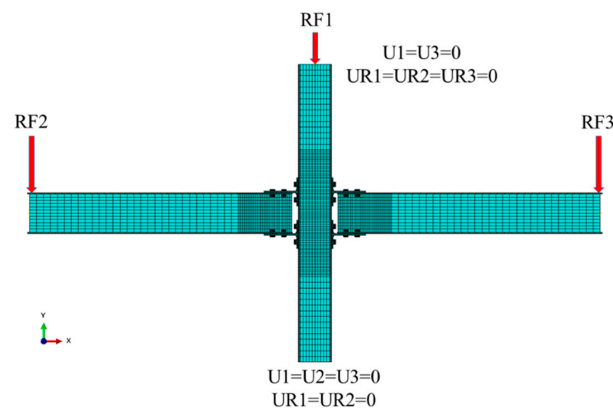
Figure 16. Finite element model.

Comparing the hysteresis curve (Figure 12), skeleton curve (Figure 13), and stiffness degradation curve (Figure 14) obtained by finite element calculation with the test results, it can be seen that the two results are consistent. Table 6 shows the main performance parameters of the finite element results and the test results. It can be seen from the table that the difference between the main performance parameters obtained by the test and the finite element results is within 20%, indicating that the finite element analysis is in good agreement with the test.

Table 6. Comparison of finite element results and test results.

Project	Fy	Fu	μ	h_e
test	23.71 [1]	67.26	2.49	0.174
finite element	28.68	75.24	2.57	0.189
differentials (%)	17.3	10.6	3.1	7.9

[1] The data in the table are averaged.

7. Strain Analysis

7.1. Overall Strain Analysis

Figure 17 shows the strain curves of the main measuring points in the test components. In the displacement control stage, the strain value at the junction of the T-shape steel web and the flange was the first to reach yield. It had high strain during subsequent loading and had the most significant plastic deformation. In addition, although the strain gauges around the bolt hole on the beam reached the yield strain value in the later loading stage, the rest of the specimen was still in the elastic stage, and there was no obvious deformation phenomenon. The above results show that the energy dissipation of such joints is mainly caused by plastic deformation of the T-shaped steel connectors under cycling loads in order to maintain the overall stability of the components.
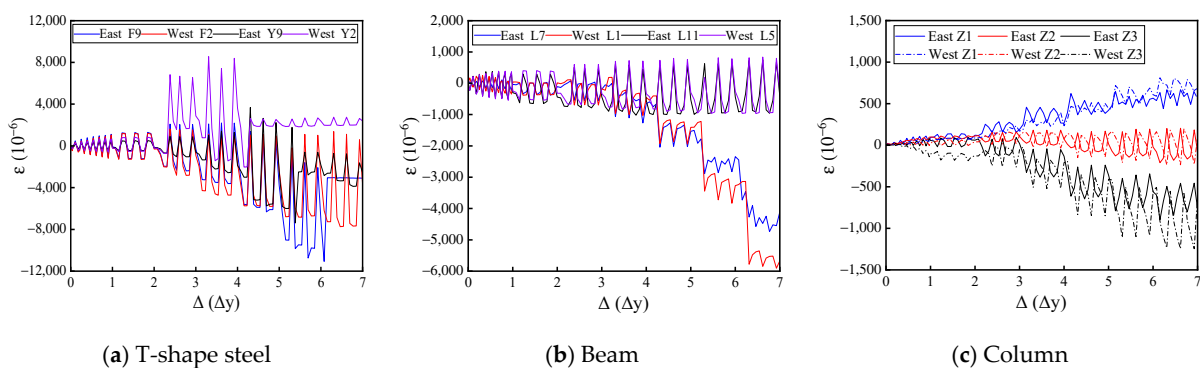

(**a**) T-shape steel (**b**) Beam (**c**) Column

Figure 17. Strain curve of main measuring points of components.

7.2. Bolt Strain Analysis

In order to intuitively monitor the strain condition of the one-side bolts in the test, an electronic strain gauge was attached to the appropriate position on the monitored one-side bolts (Figure 18). Figure 19 shows the monitored strain curve of the one-side bolts. It can be seen that the bolt strain continues to rise as the loading stage increases. In the early loading stage, the bolts' strain value increases slowly. In the third loading stage, the strain value increases significantly. This shows that the bolt has a slip tendency in the third cyclic loading stage and the applied force around the bolt hole increases gradually. When the test was at the final loading stage, the maximum strain value of the LS2 bolt on the east side of the column was 3256.2×10^{-6}, and the bolt strain did not reach yield. After the test, the bolt had no obvious plastic deformation, indicating that one-side bolts have superior performance and are suitable for this type of beam–column connection.
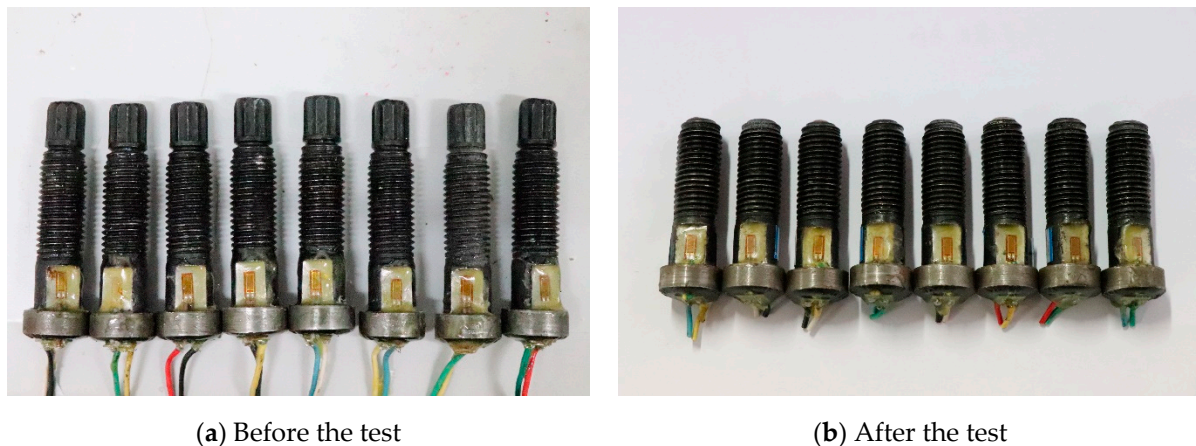

(**a**) Before the test   (**b**) After the test
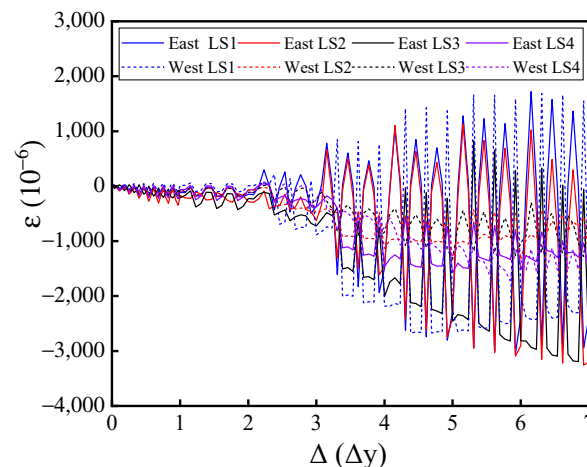
Figure 18. One-side bolt patches.

Figure 19. Strain curve of one-side bolts.

8. Conclusions

This study investigated a joint connection using one-side bolts and T-shape steel. Within the study context, the hysteresis, rotation stiffness degradation, and strain curves of the east and west beams were obtained. Based on the experimental data, this semi-rigid joint's mechanical characteristics and seismic performance were comprehensively analyzed. The following conclusions were obtained:

1. When the beam end loading method was adopted in this type of semi-rigid joint, the force and deformation of the beam ends on either side were not completely synchronous, leading to slight differences in the seismic performance between either

2. In the semi-rigid beam–column joints, with T-shape steel as the connector, the energy was mainly dissipated through plastic deformations in the T-shape steel. The plastic hinge appeared mainly at the junction of the T-shape steel web and flange, where plastic deformation was the largest;

3. The test results are in good agreement with the finite element results, which indicates that the finite element numerical analysis method can be used to study the seismic performance of the joint member;

4. The one-side bolts had superior performance and were more suitable for connecting the steel tube column-enclosed space. The strain value increased steadily during the test loading process. After the test, the yield strain was not reached, and there was no obvious plastic deformation, showing good mechanical characteristics. Therefore, it is recommended that such one-side bolts be applied in practical engineering.

References

1. Wang, X.W. *Research and Application of Mechanical Behavior of Split T-Shape Steel Beam-Column Connection*; Luoyang Institute of Technology: Luoyang, China, 2009.
2. Chang, X.; Sun, J.Q.; Wang, S.R.; Kang, A.Z.; Peng, J.C. Horizontally loaded steel pipe piles anchored in bare and hard rock under deep water condition: Parametric analysis. *Ocean. Eng.* **2022**, *266*, 112715.
3. Li, G.Q.; Duan, L.; Lu, Y.; Zhang, L.; Jiang, W.H. Bearing capacity performance of one-way bolted joints of H-shape steel beam and rectangular steel tube column flush end plate. *J. Tongji Univ.* **2018**, *46*, 162–169.
4. Li, D.S.; Tao, Z.; Wang, Z.B. Test study on static behavior of concrete-filled steel tubular column-steel beam one-side bolts connection. *J. Hunan Univ.* **2015**, *42*, 43–49. [CrossRef]
5. Jia, S.S.; Wang, Y.; Wang, X.J.; Liu, X.L. Study on seismic performance and restoring force model of one-side bolts connection between rectangular steel tube column and H-shape steel beam. *J. Build. Struct.* **2020**, *41*, 168–179. [CrossRef]
6. Liu, Y.Z.; Christian, M.C.; Ahmed, Y.E. Behavior of open beam-to-tubular column angle connections under combined loading conditions. *Steel Compos. Struct. Int. J.* **2014**, *16*, 157–185. [CrossRef]
7. Wang, W.; Li, W.; Chen, Y.; Jian, X. Cyclic behavior of endplate connections to tubular columns with novel slip-critical blind bolts. *Eng. Struct.* **2017**, *148*, 949–962. [CrossRef]
8. Zhou, S.Z.; Wu, C.F.; Sun, Q.; Zhang, W.C.; Zhang, M.; Liu, M.; Wang, P.J.; Zhao, H.; Shang, Y.W. Mechanical behavior of threaded anchored one-side bolts endplate connections between steel tubular columns and steel beams. *Dev. Build. Steel Struct.* **2021**, *23*, 22–29. [CrossRef]
9. Ban, H.Y.; Kong, S.Y.; Xie, C.F.; Wang, B.X. Study on strain relaxation and shear resistance of new high strength bolt unilateral connection. *Ind. Constr.* **2019**, *49*, 146–150+161. [CrossRef]
10. Wang, Y.; Jia, S.S.; Chai, W.J. Test study and numerical simulation of T-stub connections with one-side high-strength bolts. *J. Tianjin Univ.* **2018**, *51*, 78–85.
11. He, Z.F.; He, M.S.; Jiao, J.; Li, W.Z. Study on seismic performance of new one-side all-bolt joints and ordinary all-bolt joints. *Build. Struct.* **2017**, *47*, 63–68. [CrossRef]

12. Lee, J.; Goldsworthy, H.M.; Goldsworthy; Gad, E.F. Blind bolted moment connection to unfilled hollow section columns using extended T-stub with back face support. *Eng. Struct.* **2011**, *33*, 1710–1722. [CrossRef]

13. General Administration of Quality Supervision, Inspection, and Quarantine, Ministry of Construction of the People's Republic of China. *Steel Structure Engineering Construction Quality Acceptance Specification: GB50205—2020*; China Planning Press: Beijing, China, 2020.

14. General Administration of Housing Quality Supervision, Inspection, and Quarantine of the People's Republic of China. *Tensile Test of Metallic Materials Part 1: Test Method at Room Temperature: GB/T228.1—2010*; China Standards Press: Beijing, China, 2011.

15. Ministry of Housing and Urban-Rural Development of the People's Republic of China. *Code for the Seismic Test of Buildings JGJ/T101—2015*; China Construction Industry Press: Beijing, China, 2015.

16. Bu, X.; Gu, Q.; Wang, X.W. Test study on seismic behavior of mid-column space joints of T-shape steel beam-column connection frame. *Eng. Mech.* **2017**, *34*, 105–116.